APPLIED SCIENCES AND ENGINEERING

E. coli "super-contaminates" narrow ducts fostered by broad run-time distribution

Nuris Figueroa-Morales[1,2], Aramis Rivera[3], Rodrigo Soto[4], Anke Lindner[1], Ernesto Altshuler[5], Éric Clément[1]*

One notable feature of bacterial motion is their ability to swim upstream along corners and crevices, by leveraging hydrodynamic interactions. This motion through anatomic ducts or medical devices might be at the origin of serious infections. However, it remains unclear how bacteria can maintain persistent upstream motion while exhibiting run-and-tumble dynamics. Here, we demonstrate that *Escherichia coli* can travel upstream in microfluidic devices over distances of 15 mm in times as short as 15 min. Using a stochastic model relating the run times to the time that bacteria spend on surfaces, we quantitatively reproduce the evolution of the contamination profiles when considering a broad distribution of run times. The experimental data cannot be reproduced using the usually accepted exponential distribution of run times. Our study demonstrates that the run-and-tumble statistics determine macroscopic bacterial transport properties. This effect, which we name "super-contamination," could explain the fast onset of some life-threatening medical emergencies.

INTRODUCTION

Bacteria live in a wide variety of natural environments in which fluid flow is present, including the capillary networks of animals and plants and porous soils (*1*, *2*). Upstream bacterial infections often occur in ducts where liquids are oscillating or flowing in one direction, such as in the human urinary tract and medical catheters (*3*–*5*). Understanding the upstream motility of bacteria in such confined scenarios is crucial to prevent infections or control microbial soil pollution (*6*).

An extended motility mechanism in bacteria in open environments is the well-known run-and-tumble dynamics (*7*). In this strategy, the cells moves in a series of straight paths with quick reorientations of the swimming direction, resulting in 3D random walks (*7*). Solid surfaces modify the bacterial dynamics, introducing hydrodynamic interactions that lead to surface accumulation and circular trajectories (*8*, *9*). Increased complexity emerges in shear flows, from the interplay between the flow and confining surfaces and the bacterial structures (fore-aft asymmetry and chiral flagella) (*10*–*12*). At low shear rates, bacteria can migrate upstream close to the surfaces and the edges of the bounding structures (*10*, *12*–*16*). High shear rates, on the other hand, produce an erosive detachment (*16*) from the surfaces. The overall transport in a confined channel is then built on diverse contributions: downstream advection in the bulk and, depending on the flow velocity, upstream and/or downstream motion along the crevices and close to the surfaces.

Despite its potential importance, to our knowledge, typical distances for upstream swimming have not been previously determined. Hydrodynamic interactions between the swimmer and the surface are related to the velocity and geometry of the swimmer (*8*). For a bacterium undergoing tumble, the hydrodynamic interactions will

be decreased, and the erosion process enhanced. On this logic, the statistics of tumbles and runs should critically determine the upstream bacterial contamination inside microchannels.

For *Escherichia coli*, the run-time distribution was reported to follow a single-time exponential process related to the rotational switching of the flagellar motor (*17*). More recently, direct measurements on flagellar motors show heavy-tailed distributions of rotation times stemming from the intrinsic noise in the chemotactic signaling (*18*). Experimental works highlight the existence of very persistent trajectories in swimming bacteria (*19*–*21*) or swarms displaying anomalous Levy walk migration (*22*), possibly connected to a heavy-tailed distribution of run times. However, most theoretical or numerical studies use an exponential process to model the microscopic stochasticity of the kinematics (*23*). The influence of these stochastic processes on the macroscopic bacterial transport remains an open question (*21*, *24*, *25*).

Here, by means of a video scanning technique, we study the upstream migration of *E. coli* with single-bacteria resolution up to macroscopic distances in excess of 15 mm. We find that the contamination takes place in the form of a front of invading bacteria, moving upstream along surfaces and corners, with a front velocity almost independent of the perfusion fluid velocity—we call it "super-contamination." We found this process to be related to the existence of very long run times.

When the time that bacteria spend close to surfaces is linked to the run times and the duration of runs is modeled by a broad distribution, we find a quantitative agreement with the experimental spatiotemporal dynamics. However, exponentially distributed run times fail to even qualitatively describe this process. This effect may explain several acute medical problems, such us fast infections in the urinary tract or through medical catheters.

RESULTS

Experiments

The experimental setup, as sketched in Fig. 1A, consists of a few-millimeter-long polydimethylsiloxane (PDMS) rectangular channel of width $w = 40$ μm, height $h = 11$ μm, and length $L = 15$ mm, glued

[1]Laboratoire de Physique et Mécanique des Milieux Hétérogènes, PMMH, ESPCI Paris, PSL University, CNRS, Sorbonne Université, Université de Paris, 75005 Paris, France. [2]Department of Biomedical Engineering, The Pennsylvania State University, PA 16802, USA. [3]Zeolites Engineering Lab, IMRE, University of Havana, 10400 Havana, Cuba. [4]Departamento de Física, FCFM, Universidad de Chile, Santiago, Chile. [5]Group of Complex Systems and Statistical Physics, Physics Faculty, University of Havana, 10400 Havana, Cuba.
*Corresponding author. Email: eric.clement@upmc.fr
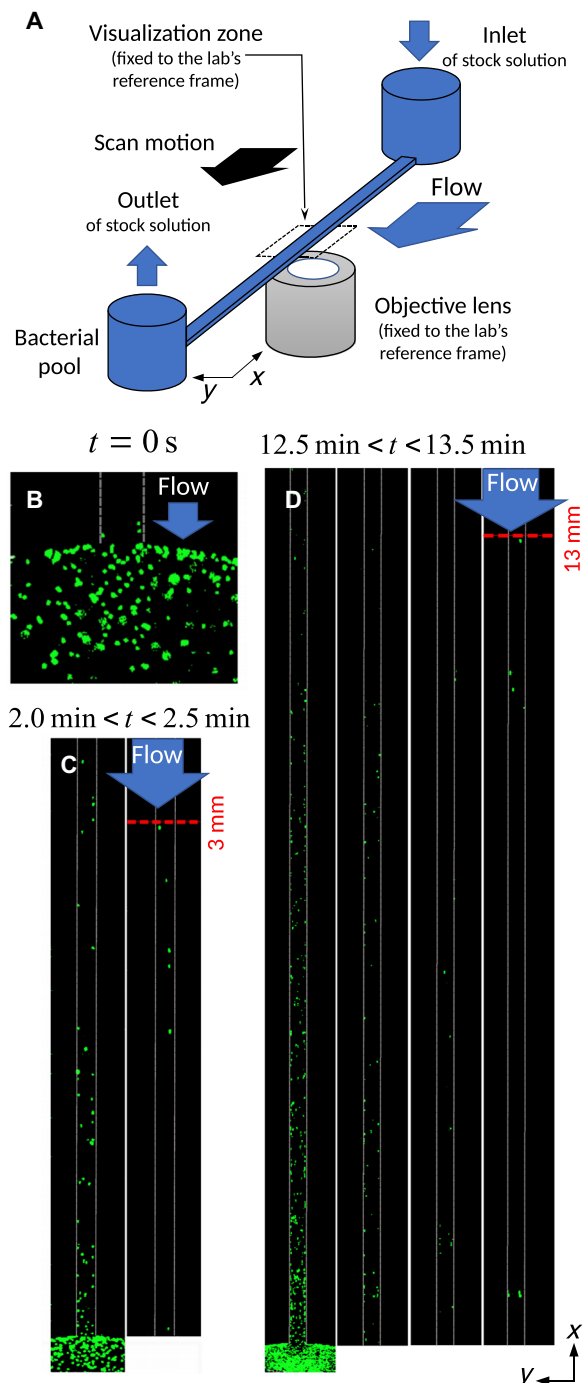
Fig. 1. Visualizing upstream super-contamination. (**A**) Sketch of the microfluidic device. The black arrow indicates the direction of motion of the setup during a scan, while the lens stays in place. (**B**) Image of swimmers, represented by green spots, near the exit of the bacterial reservoir at the beginning of one contamination experiment. (**C**) Reconstruction of the channel using images from a scan performed between 2 and 2.5 min from the beginning of the experiment: The pioneer swimmer has reached a distance of 3 mm from the bacterial reservoir. (**D**) An analogous reconstruction, taken from a scan performed from 12 to 13.5 min: The pioneer swimmer has reached a distance of 13 mm. The flow velocity at the center of the channel was 80 μm/s. As a size reference, the width of the channel is $w = 40$ μm.

on top of a PDMS-covered glass slide. Its extremes end up in two cylindrical reservoirs of 1-mm diameter, connected to tubing that allows fluids to circulate using a gravity flow.

At the beginning of the experiment, the outlet reservoir is filled with *E. coli* bacteria (strain RP437 expressing green fluorescent protein). For every experiment, the average bacterial velocity in the reservoir V_{br} is measured. By injecting a sufficiently high flow rate of the fluid without bacteria through the inlet, bacteria are kept in the outlet reservoir, not yet invading the channel. See Materials and Methods for details on the procedure. Then, at $t = 0$, a controlled flow of the bacteria-free liquid is established from the inlet to the outlet, and the system is video recorded. Bacteria start swimming upstream along the channel. The flow rate in the channel is determined by tracking passive latex beads suspended in the perfusion fluid. The maximum flow velocity measured in the center of the channel is represented as V_f ($0 \leq V_f \leq 80$ μm/s). Since our experimental conditions avoid the presence of chemical gradients, our experiment is different from those of (*26*) and (*27*).

To visualize individual bacteria over the macroscopic extent of the channel, which is several millimeters long starting from the outlet reservoir, we translate the channel at a constant velocity $V_s = 150$ μm/s along the $-x$ direction, while a video is taken through an inverted microscope fixed on the laboratory reference frame (Fig. 1A). The channel is scanned several times during a single experiment at a fixed flow rate. Movie S1 shows a sequence of three scans starting at different times during the same experiment.

Figure 1 (B to D) shows a combination of images taken during scans starting at different time points. The total time interval associated with one image spans from the beginning of the scan to the moment of visualization of the farthest bacteria from the reservoir, which we call "pioneers." There, we visualize all the bacteria along the channel length, independently of their vertical position. The multiple side-by-side images in Fig. 1 (C and D) are actually end-to-end in the physical system. Note that this channel reconstruction does not constitute a snapshot, since different segments display the conditions at different instants. However, the pictures demonstrate the arrival of bacteria as far as 13 mm from the bacterial reservoir in 13.5 min. This constitutes direct evidence for the ability of bacteria to swim upstream over macroscopic distances in a short time interval.

In Fig. 2A, we display details of the trajectories of some bacteria near the outlet (the bacterial reservoir). Figure 2B is a zoom illustrating how the flow (approximately five at the center of the channel) induces the bacteria to concentrate near the entrance of the channel. This is associated with bacteria attaching and detaching from the walls of the reservoir and moving progressively toward the channel, a phenomenon previously reported using a funnel geometry (*14*). This densification at the outlet creates favorable conditions to prime an efficient contamination process in the channel, as it will induce higher chances for the bacteria to get inside the microchannel via upstream swimming close to surfaces but mostly along the channel edges. This last phenomenon is illustrated by the vertical trajectories in the picture. The red arrows indicate a typical contaminating trajectory: After swimming upstream along the left wall of the channel, the bacterium is detached from it, and then, it is advected downstream and reattaches to the right wall of the channel, continuing its upstream motion. After many events like this, our persistent swimmer eventually reaches the opposite extreme of the channel. That event is illustrated in Fig. 2C, where the bacterial trajectory is pointed out by red arrows, while the orange arrows
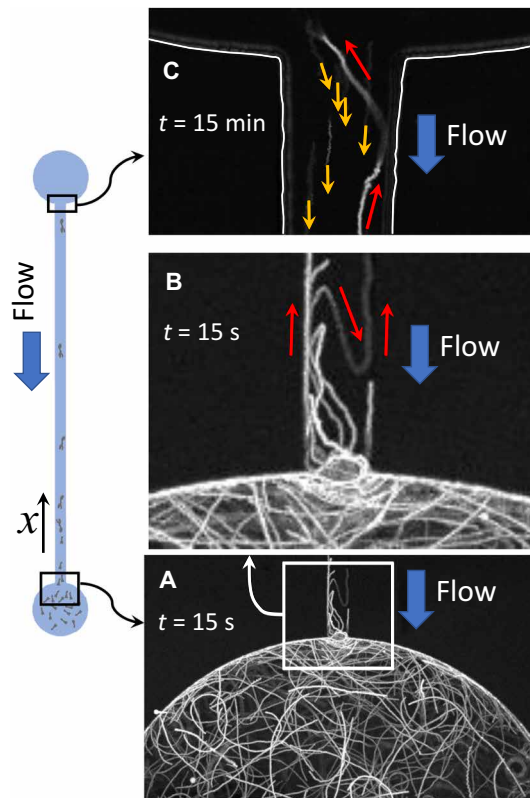
Fig. 2. Bacterial paths represented by the superposition of photograms on fixed positions. Individual images were taken at intervals of 1/30 s from a 13-s-long video for (**A**) and (**B**), and 9-s-long video for (**C**). (A) Bacterial trajectories near the entrance of the channel from the bacterial reservoir, 15 s after starting the contamination experiment. (B) Zoom at the entrance of the channel: Red arrows indicate the path of one bacterium that first moves upstream along the left wall, then detaches from it, and then reattaches to the right wall, continuing its upstream motion. (C) A zoom at the end of the channel: Red arrows indicate the upstream trajectory of a bacterium that has reached the opposite extreme of the channel after swimming for a distance bigger than 15 mm in 15 min; the orange arrows indicate the paths of "inactive" beads moving downstream (the borders of the channel have been overdrawn in white for clarity). The flow velocity at the center of the channel was of 5 μm/s. As a reference, the width of the channel is $w = 40$ μm.

indicate the motion of tracer latex beads used to determine the flow rate.

On Fig. 3A, we show, for two experiments at different flow velocities V_f, the scanning position as a function of time, until the farthest contaminating bacteria are found. The lines topping the scanning positions highlight the advance of those individuals, which we define as pioneers. Notably, these are straight lines (Fig. 3B), indicating that the pioneer contamination front advances at constant speed, V_{cont}. With the scanning technique, it is not possible to detect whether the pioneering bacteria hence identified remain the same or if there is a group of pioneers alternating the leading position. However, the tracks on Fig. 2 suggest that the second scenario is more plausible. The simulations of the model described later also support the idea that different bacteria take the pioneer role at different moments.

In Fig. 3C, we display the ratio between V_{cont} and the average bacterial velocity in the reservoir, V_{br}, as a function of the flow rate. At zero flow, the velocity is highest, as expected. However, although

we have large data scattering for the finite flow range explored, we cannot see any systematic variation with V_f. We think that it may be related to the large variation of bacterial velocities between experiments. In the experiment where $V_f = 65$ μm/s (average shear rate, 11.0 s^{-1}) bacteria advance upstream at the large velocity $V_{cont} = 39$ μm/s (2.3 mm/min). In the case $V_f = 80$ μm/s (nearly four times the average bacterial velocity; average shear rate, 13.6 s^{-1}), the pioneer bacterial front advances at nearly $V_{cont} = 15$ μm/s (0.9 mm/min).

It is worth noting that the advance of the pioneer contaminants should ultimately depend on the dispersion of the velocity distribution of the bacteria. The pioneers are likely to be the fastest and more persistent among the population, whereas the upstream contamination is a phenomenon involving the whole bacterial population. To gain insight into the phenomenon, we analyze the concentration profiles that can be reconstructed from scans (see Materials and Methods for details). Figure 4 (A and B) illustrates these profiles for two different experimental conditions.

**Modeling upstream super-contamination**

Now, we analyze the microscopic mechanisms responsible for the upstream super-contamination. At low flow, the process takes place due to the upstream swimming of bacteria along edges and surfaces and only along the edges for higher fluid velocities (16). When bacteria leave the wall interceptions or the surfaces, they are transported downstream. These advected bacteria eventually reattach on the surfaces and again start their upstream migration as in Fig. 2 (13, 14, 16). This upstream-downstream dynamics is shown in movie S2 and Fig. 5A, which displays the trajectories of some bacteria taken from the video.

We propose to model the upstream transport process using a simple one-dimensional (1D) biased random walk. A given bacterium performs an upstream displacement l, until it detaches from the wall. Then, it will be transported downstream a fixed distance d, until it reattaches to the surface, starting its upstream swimming again. Figure 5B shows a diagram synthesizing these ideas. Our key hypothesis is that the passage from upstream to downstream motion is controlled by the occurrence of tumbling events, where bacteria cease swimming and debundle their flagella. Since the attraction at surfaces and borders is a generic result of hydrodynamic interactions between pusher-swimmers and solid boundaries (8), it is not present when bacteria stop swimming. Therefore, a tumbling bacterium would likely lose the attraction forces to the surface and then be carried downstream by the flow. Under flow, the detachment probability was found to increase leading to a shear-mediated erosion as observed in (16). However, the characteristic shear rates for erosion from surfaces and edges are rather high (140 and 250 s^{-1}, respectively) (16). It is then reasonable to consider that at the low shear rates of our experiments, desorption is essentially caused by tumbling events. In this picture, the distance l is a random variable; hence, the contamination process should depend critically on the detailed statistics of the run-and-tumble events.

In the pioneering work of Korobkova et al. (18), the motor switching statistics were measured for individual bacteria. The duration of the counterclockwise state of the motors (which is related to the run mode of bacteria) was found to be widely distributed, as opposed to a simple exponential process often put forward to describe bacterial motility (17). To decipher the role of the run-time distribution on the contamination process, we present in our analysis two parallel approaches, one using a broad distribution illustrated by a power law ψ_{PL}, from the single flagellum statistics (18), and a
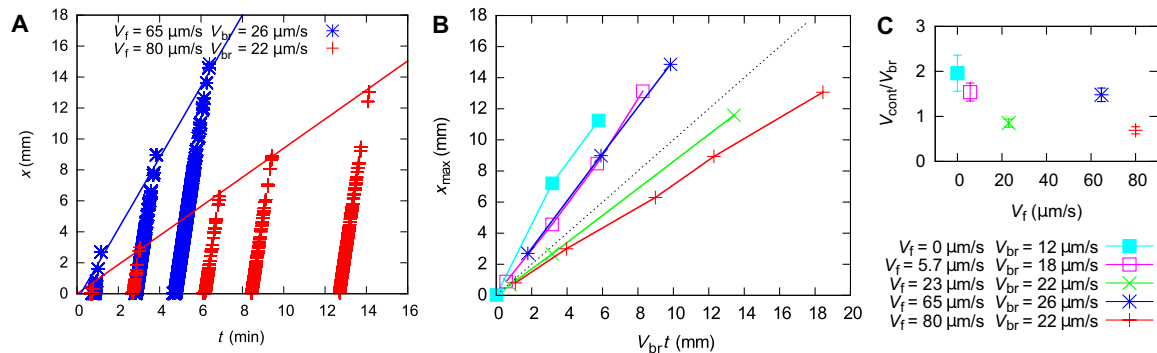
Fig. 3. Quantification of the upstream pioneer contamination. (**A**) Scanning position (crosses) for two experiments with different flow velocities. The scanning stops at the farthest bacteria (pioneers). The straight lines show the advance of the contamination pioneers, with a slope that gives the contamination velocity V_{cont}. (**B**) Positions of the pioneers as a function of $V_{\text{br}}t$. The dotted line is the curve $y = x$. (**C**) $V_{\text{cont}}/V_{\text{br}}$ as a function of V_{f} for different experiments.
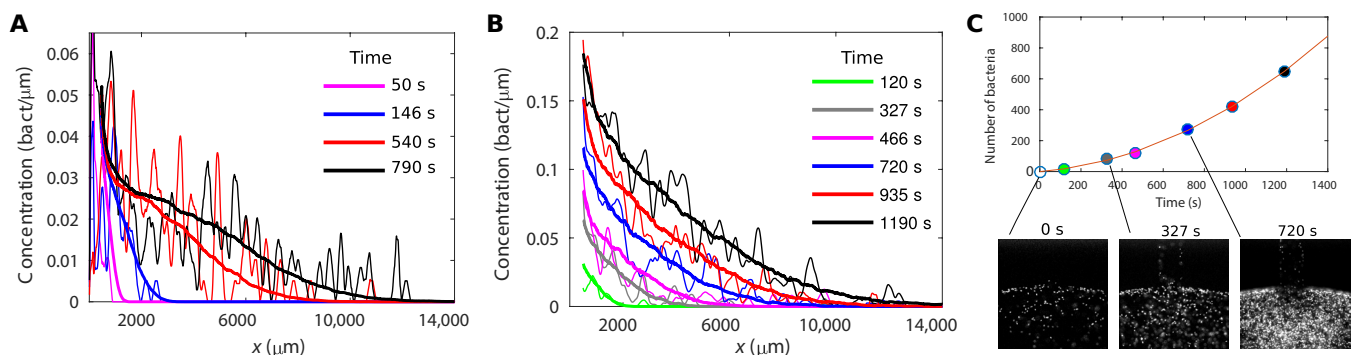
Fig. 4. Concentration profiles and boundary conditions. (**A**) and (**B**) show the concentration profiles along the channel at different times, for two different flows: $V_{\text{f}} = 23\ \mu\text{m/s}$ and $V_{\text{f}} = 80\ \mu\text{m/s}$, respectively. The average bacteria velocity in the reservoir is $V_{\text{br}} = 22\ \mu\text{m/s}$ in both cases. The thicker continuous lines are simulations based on the broad statistical distribution of run times ($\alpha = 0.5$ and $V_b = 22.0\ \mu\text{m/s}$) for (A) and ($\alpha = 0.5$ and $V_b = 19.5\ \mu\text{m/s}$) for (B). (**C**) Number of bacteria inside the channel for the set of scans of (B), using the same color code. The three snapshots show the increase in the concentration in the outlet (stock of bacteria) as time goes, therefore increasing the flux of bacteria into the channel.

second using an exponential distribution ψ_P of run times (*17*). To model the broad distribution, we use the probability distribution of run times $\psi_{\text{PL}}(t) = \gamma/[\tau_0(1 + t/\tau_0)^{\gamma+1}]$, with $\tau_{\text{run}} = \tau_0/(\gamma - 1)$. The parameters used are $\tau_0 = 1$ s and $\gamma = 1.2$ ($\tau_{\text{run}} = 5$ s) corresponding to the measurements performed on individual flagellar rotations (*18*). The corresponding distribution in the exponential case is $\psi_P(t) = \frac{e^{-t/\tau_P}}{\tau_P}$, with $\tau_{\text{run}} = 1$ s, a classical value describing the run-and-tumble process for wild-type *E. coli*. From this, we can estimate the average upstream swimming distance $\langle l \rangle$ as the upstream bacterium velocity V_b times the average run time τ_{run}. To render the efficiency of the tumble process to produce desorption, it is possible to define a parameter p_e equal to the probability of a tumble to be effective, i.e., to remove the bacteria from the surface. This would lead to $\langle l \rangle = V_b\tau_{\text{run}}/p_e$.

We now define a dimensionless parameter quantifying the contamination, $\alpha = d/\langle l \rangle = p_e d/(V_b\tau_{\text{run}})$. When $\alpha \ll 1$, the persistent upstream motion dominates and upstream contamination takes place. On the other hand, when $\alpha \sim 1$, the contamination will be slow since bacteria will be transported downstream almost as much as they can swim upstream between successive detachments. For $\alpha > 1$, no contamination occurs.

It should be underlined that for times larger than τ_{run}, running a simulation with some values of d and p_e is equivalent to considering that all tumble events are effective (i.e., $p_e = 1$) but the downstream traveled distance would then be reduced to the value $p_e d$. There-

fore, for simplicity, in the simulations, we use $p_e = 1$, and the stochastic biased random walk model is only controlled by a single dimensionless parameter α. The average run time τ_{run} and the bacteria velocity V_b fix the time and length units when comparing simulations and experiments. Other parameters can be absorbed into α. (Note that although all the physical magnitudes and expressions have been defined in the text, table S1 shows a compilation of the definitions used).

The distribution of d is difficult to evaluate quantitatively because, for many bacteria, most subsequent detachment or reattachment events do not lie within the visualization window. However, for the flow of Fig. 5A, we could identify some events and evaluate d to be of the order of tens of micrometers. Once the value of τ_{run} is chosen from the first moment of the chosen run-time distribution, the experiment can be fitted by two free parameters: V_b and α.

We simulate the trajectories of individual bacteria undergoing upstream and downstream flow transport, according to the hypotheses of the model. Detachments from the walls are obtained via a Monte Carlo dynamics following different statistics for the run times. To illustrate the strong qualitative differences between the contamination processes for the classical exponential process and the power-law distribution, we present in Fig. 5 (C and D) simulated contamination curves. To produce those plots, many bacterial trajectories were generated using a constant flow rate boundary condition at the outlet,
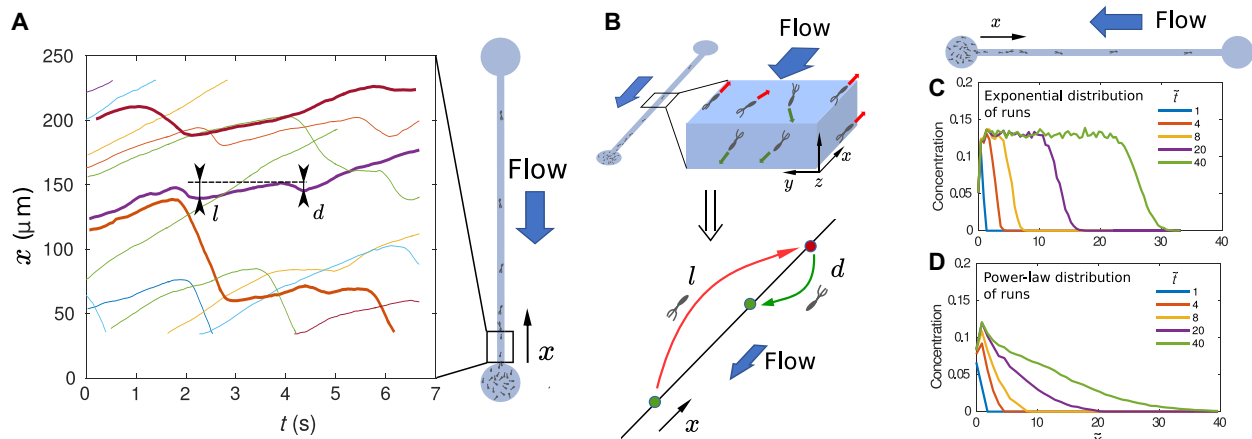
Fig. 5. Modeling super-contamination. (**A**) Experimental spatial-temporal plot illustrating the two characteristic lengths associated with the upstream bacterial motion. (**B**) Sketch showing the mechanism of upstream contamination in 3D (top) and in the 1D version, supporting a biased random walk model (bottom). (**C** and **D**) Contamination profiles at different times generated by the biased random walk model based on exponential and broad distributions of run times, respectively. The flux of bacteria from the reservoir was kept constant in the simulations. The dimensionless time and length scales make the profiles good for comparison.

i.e., bacteria entering in the channel at a constant rate. From the accumulation of all the tracks, one determines the simulated spatial concentration profiles at different instants. In these curves, we normalized the time scale by the mean run time τ_{run} and the spatial scale by $V_{\mathrm{b}}\tau_{\mathrm{run}}$. The results can now be compared, which turns out to be different for the two distributions. In the exponential case (Fig. 5C), one observes steep fronts moving upstream. In the power-law case (Fig. 5D), the concentration profiles have very long tails composed of a few very persistent upstream swimmers.

To perform a full comparison with the previous set of experiments, another crucial feature must be taken into account. Notably, the bacteria concentration displays a steady increase in the reservoir [see Fig. 4 (A and B) and the snapshots of Fig. 4C for the set of scans reported in Fig. 4B]. Bacteria come swimming upstream through the outlet tube, where the dimensions are big compared to the microfluidic channel. Once in the outlet reservoir, only a small fraction of bacteria swim upstream in the thin microchannel, and the concentration in the reservoir builds up. This effect imposes nonsteady boundary conditions at the outlet, which should be explicitly taken into account in the quantitative evaluation of the model. To address this issue, we count the total number of bacteria inside the channel for every scan $N_{\mathrm{b}}(t)$ (shown in the plot of Fig. 4C). The flux of bacteria into the channel is simply dN_{b}/dt, which is fitted by a quadratic function and used as a nonsteady boundary condition in the simulations.

For every run of the simulations, using parameters (V_{b}, α), we define a quality factor $F(V_{\mathrm{b}}, \alpha)$. $F(V_{\mathrm{b}}, \alpha)$ is computed as the mean squared difference between the experimental and the simulation profiles, considering all the available concentration curves at different times. The details are in the Supplementary Materials. To find the optimal parameters for a given experiment, we generate a set of numerical curves in the (V_{b}, α) space. The optimal parameters yield the minimal value of F. To compare the relevance of the two different models of run-time distribution, ψ_{PL} and ψ_{P}, one needs to compare their respective quality factor plots $F_{\mathrm{PL}}(V_{\mathrm{b}}, \alpha)$ and $F_{\mathrm{P}}(V_{\mathrm{b}}, \alpha)$.

In Fig. 4 (A and B), we display two contamination profiles obtained for bacteria of similar activity (mean velocity in the reservoir V_{br} = 22 μm/s) but for two different flow rates. The simulations Fig. 4A
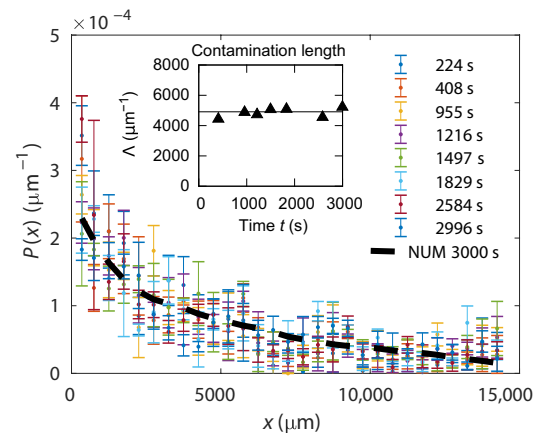
Fig. 6. Channel contamination in absence of a flow. Normalized spatial concentration $P(x, t) \equiv c(x, t)/\int c(y, t)dy$ of the bacteria in the channel, for time spanning between 400 and 3000, where $c(x, t)$ are the concentration profiles. The black line is the result of a numerical random walk model using the switch time distribution $\psi_{\mathrm{PL}}(t)$. Inset: Contamination lengths, $\Lambda(t) = \int x\, P(x, t)dx$, for the experiment and the numerical model at t = 3000 s.

correspond to an upstream bacterial velocity chosen to match the velocity measured in the reservoir ($V_{\mathrm{b}} = V_{\mathrm{br}}$ = 22 μm/s). The free parameter α = 0.5 provides the best fit. Qualitatively, the agreement is very good, as it simultaneously fits the concentrations at different times. In Fig. 4B, we show the simulations using the optimal pair of parameters V_{br} = 19.5 μm/s and α = 0.5, with a very good agreement between experiment and simulation. In both cases (Fig. 4, A and B), the optimal values of upstream velocity are very close to the bacterial velocity measured in the reservoir. We show details of the optimization maps in the Supplementary Materials, for both the power law and the exponential model. In all experiments, the exponential distribution of run times ψ_{P} fails to reproduce the spatiotemporal profiles.

For consistency, we now question the results of the contamination process in absence of flow. The contamination profiles remains essentially localized near the outlet (see Fig. 6). The observed stationary profile stems from the balance between the invasion from the outlet

reservoir and the probability to leave the channel after a while by one of the two opposite reservoirs. As soon as the flow is turned on, the situation changes markedly: Bacteria reorient toward the upstream inlet, leading to the super-contamination process. At zero flow, the first moment of the distribution characterizes a typical penetration length over a distance $\Lambda \approx 5$ mm after few minutes (Fig. 6, inset). We simulated a 1D random walk with a probability to change the swimming directions simply triggered by the broad distribution $\psi_{PL(t)}$. For a constant contamination flux of bacteria at the outlet, using a swimming velocity $V_b = 20$ μm/s and a channel of dimension $L = 15$ mm, we obtain a distribution reaching a stationary profile, once again, in quantitative agreement with the experimental measurements (see Fig. 6).

DISCUSSION

We showed in a simple microfluidic experiment that bacteria can rapidly contaminate initially clean environments by propagating upstream in a narrow channel, over long distances and for a substantial range of flow rates. We found bacteria pioneering the contamination that are capable of swimming upstream at average constant velocity over distances in excess of 1 cm. Furthermore, the contamination process shows long-tailed profiles populated by bacteria persistently moving upstream, which constitutes the signature of super-contamination.

Solving numerically a simple 1D model of biased random walk, we quantitatively related the spatiotemporal contamination profiles to the underlying presence of a broad run-time distribution stemming from the clockwise/counterclockwise statistics of the bacterial motor rotation. On the other hand, the simple exponential distribution for run times that would be associated with a Poisson distribution of run times is not able to reproduce the contamination profiles. To our knowledge, we make a quantitative relation between single-cell experiments on bacterial motors and the outcome of a macroscopic transport process. This puts forward that singular features of the run-and-tumble statistics, born in the stochasticity in the chemotactic circuitry, have a definite influence on macroscopic transport, in agreement with recent observations from 3D Lagrangian tracking (20, 21).

In practice, our measurements suggest that swimming bacteria can overcome distances comparable to the sizes of animal organs (tens of centimeters) in some tens of minutes or a few hours under conditions of high confinement. In the human urinary tract, for example, ureters are tubes with muscular walls that undergo successive waves of active muscular contraction to move liquid from the kidney to the bladder. When totally contracted, it collapses to a slit-shaped, very confined cross section, possibly favorable to upstream bacterial migration. When fully distended, we estimate shear rates of around 10 to 60 s^{-1} (28). At these low shear rates, bacteria undergo little erosion from surfaces and edges (16). Contamination fronts advancing at 15 to 25 μm/s could overcome the length of the ureters (200 to 300 mm) and travel from the bladder to the kidneys in 3 to 7 hours, possibly starting a renal infection.

The super-contamination could be relevant in other scenarios: Histological studies of the bovine cervical mucosa showed longitudinal grooves of cervical folds, which maintained continuity throughout the cervix (29). These geometrical conditions potentially facilitate the fast upstream migration of bacteria with a subsequent infection. Acute cholangitis, another medical emergency, is usually caused by bacteria ascending from the duodenum through the bile duct and infecting it (30), especially when it is partially obstructed and therefore provides a very confined environment ideal for upstream contamination.

MATERIALS AND METHODS
Bacterial strains and culture
We use wild-type RP437 *E. coli* bacteria. The cells are cultured overnight at 30°C in M9 minimal medium supplemented with casamino acids (1 mg/ml) and glucose (4 mg/ml). Next, bacteria are washed twice by centrifugation (2300g for 5 min), and the cells are resuspended into a motility medium containing 10 mM potassium phosphate (pH 7.0), 0.1 mM K-EDTA, 34 mM K-acetate, 20 mM sodium lactate, and 0.005% polyvinylpyrrolidone (PVP-40). In this medium, bacteria remain motile but do not divide.

Microfluidic device and procedure
The experimental cell is a microfluidic channel (rectangular cross section; width $w = 40$ μm, height $h = 11$ μm, and length $L = 15$ mm) ended with two large cylindrical reservoirs. The microfluidic cell is made in PDMS using a conventional soft photolithography technique and assembled onto glass plates previously coated with a thin layer of PDMS. Stainless steel tubes of 1-mm diameter were inserted at each end of the channel in the cylindrical reservoirs, connected to large liquid containers through plastic flexible tubes. After a full filling of the microfluidic system with the stock solution without bacteria, the metallic connector from the outlet was replaced by a similar one connected to a big container containing the same liquid as the inlet, as well as bacteria. As a result, we start the experiment with a bacterial suspension located at the left end of the channel (see the panel corresponding to $t = 0$ in Fig. 1), while the rest of its length was filled with a bacteria-free medium. The microfluidic channel is placed on an inverted microscope (Zeiss Observer Z1) equipped with an xy mechanically controllable stage from Applied Scientific Instrumentation (ASI), a digital camera [ANDOR iXon 897 electron multiplying charge-coupled device (512 pixels by 512 pixels) at a frequency of $f = 30$ fps (frames/s)] with a ×40 magnification objective.

Flow is established by imposing a small height difference between the two large containers on both sides of the channel, which allows us to work at very small flow rates. We visualize all the bacteria along the microchannel height by epifluorescence. As time passes by, bacteria migrate upstream along the channel. A single realization of the contamination experiment consists in performing periodic scans along the whole channel length. The microscope stage is displaced along the channel axis at a scanning velocity of $V_s = 150$ μm/s while recording a video. Bacterial positions are then determined, and by image postprocessing, we relate the number of bacteria in each frame to its distance x from the reservoir.

Between subsequent scans, a video is taken at a fixed position using direct light illumination, thus enabling the visualization of latex bead tracers. The velocity profile was determined for each applied pressure difference, through the beads velocities in the flow.

Construction of the bacterial concentration profiles along the channels
To obtain the contamination profiles from the scans, we count the number of bacteria in each frame. Since the distance between two consecutive pictures, $\Delta x_s = V_s/f = 150$ μm/s per 30 fps = 5 μm, is

smaller than the piece of the channel imaged in one frame ($L_x = 160$), some bacteria are imaged several times. To obtain a concentration profile, we normalize the total number of bacteria detected by the average number of times that a bacterium was recorded: $L_x/\Delta x_s$. As the profiles do not come from snapshots but from scans, they are naturally stretched, showing tails longer than what they really are. We correct for the stretching as follows: Consider a bacterium in the position $x > 0$ at the starting moment of the scan and swimming upstream with a speed V_b. This bacterium will be registered at the moment $t > 0$ when it has traveled a distance $\Delta x = V_b t$. In the reference frame of the channel, the objective, initially at $x = 0$, would have traveled a distance $x_m = x + \Delta x = V_s t$ when it captures the bacterium. Here, V_s is the scanning velocity ($V_s > V_b$). From the equality of times, we obtain $\frac{\Delta x}{x_m} = \frac{V_b}{V_s}$, which shows that the deformation is linear with the distance to the reservoir. In our experiments the coefficient is in the range of $0.02 < \frac{\Delta x}{x_m} < 0.2$. With this principle, we rescaled the x axis to reduce the profile stretching. The new x values are $x = x_m - \Delta x = x_m\left(1 - \frac{V_b}{V_s}\right)$, where x_m is the measured coordinate from the scan.

SUPPLEMENTARY MATERIALS

Supplementary material for this article is available at http://advances.sciencemag.org/cgi/content/full/6/11/eaay0155/DC1

Fig. S1. Optimization factor F as a function of the parameters α and V_b of the model.
Fig. S2. Superposition of contamination experiments (thin lines) and simulations (thick lines) using the exponential statistics for bacterial detachments from the surfaces.
Table S1. Summary of physical magnitudes.
Movie S1. A sequence of three scans starting at times 0, 327, and 719 s for a contamination experiment with a maximum flow velocity of 80 µm/s.
Movie S2. Bacterial upstream-downstream dynamics for a contamination experiment with a maximum flow velocity of 80 µm/s.

REFERENCES AND NOTES

1. F. J. Valdés-Parada, M. L. Porter, K. Narayanaswamy, R. M. Ford, B. D. Wood, Upscaling microbial chemotaxis in porous media. *Adv. Water Resour.* **32**, 1413–1428 (2009).
2. A. Duchesne, G. Wang, G. Gülez, D. Or, B. F. Smets, Hydration-controlled bacterial motility and dispersal on surfaces. *Proc. Natl. Acad. Sci. U.S.A.* **107**, 14369–14372 (2010).
3. K. J. Wright, P. C. Seed, S. J. Hultgren, Uropathogenic *Escherichia coli* flagella aid in efficient urinary tract colonization. *Infect. Immun.* **73**, 7657–7668 (2005).
4. K. Dohnt, M. Sauer, M. Müller, K. Atallah, M. Weidemann, P. Gronemeyer, D. Rasch, P. Tielen, R. Krull, An in vitro urinary tract catheter system to investigate biofilm development in catheter-associated urinary tract infections. *J. Microbiol. Methods* **87**, 302–308 (2011).
5. H. J. Kim, D. Huh, G. Hamilton, D. E. Ingber, Human gut-on-a-chip inhabited by microbial flora that experiences intestinal peristalsis-like motions and flow. *Lab Chip* **12**, 2165–2174 (2012).
6. R. Rusconi, R. Stocker, Microbes in flow. *Curr. Opin. Microbiol.* **25**, 1–8 (2015).
7. H. C. Berg, *E. coli in Motion* (Springer, 2004).
8. A. P. Berke, L. Turner, H. C. Berg, E. Lauga, Hydrodynamic attraction of swimming microorganisms by surfaces. *Phys. Rev. Lett.* **101**, 038102 (2008).
9. E. Lauga, W. R. DiLuzio, G. M. Whitesides, H. A. Stone, Swimming in circles: Motion of bacteria near solid boundaries. *Biophys. J.* **90**, 400–412 (2006).
10. T. Kaya, H. Koser, Direct upstream motility in *Escherichia coli*. *Biophys. J.* **102**, 1514–1523 (2012).
11. Marcos, H. C. Fu, T. R. Powers, R. Stocker, Bacterial rheotaxis. *Proc. Natl. Acad. Sci. U.S.A.* **109**, 4780–4785 (2012).
12. A. J. T. M. Mathijssen, N. Figueroa-Morales, G. Junot, É. Clément, A. Lindner, A. Zöttl, Oscillatory surface rheotaxis of swimming *E. coli* bacteria. *Nat. Commun.* **10**, 3434 (2019).
13. J. Hill, O. Kalkanci, J. L. McMurry, H. Koser, Hydrodynamic surface interactions enable *Escherichia coli* to seek efficient routes to swim upstream. *Phys. Rev. Lett.* **98**, 068101 (2007).
14. E. Altshuler, G. Miño, C. Pérez-Penichet, L. del Río, A. Lindner, A. Rousselet, E. Clément, Flow-controlled densification and anomalous dispersion of *E. coli* through a constriction. *Soft Matter* **9**, 1864–1870 (2013).
15. N. Figueroa-Morales, E. Altshuler, A. Hernández-García, A. Lage-Castellanos, E. Clément, Two-dimensional continuous model for bacterial flows through microfluidic channels. *Rev. Cub. Fis.* **30**, 3 (2013).
16. N. Figueroa-Morales, G. L. Miño, A. Rivera, R. Caballero, E. Clément, E. Altshuler, A. Lindner, Living on the edge: Transfer and traffic of *E. coli* in a confined flow. *Soft Matter* **11**, 6284–6293 (2015).
17. H. C. Berg, D. A. Brown, Chemotaxis in *Escherichia coli* analysed by three-dimensional tracking. *Nature* **239**, 500–504 (1972).
18. E. Korobkova, T. Emonet, J. M. G. Vilar, T. S. Shimizu, P. Cluzel, From molecular noise to behavioural variability in a single bacterium. *Nature* **428**, 574–578 (2004).
19. M. Wu, J. W. Roberts, S. Kim, D. L. Koch, M. P. DeLisa, Collective bacterial dynamics revealed using a three-dimensional population-scale defocused particle tracking technique. *Appl. Environ. Microbiol.* **72**, 4987–4994 (2006).
20. N. Figueroa Morales, "Active bacterial suspensions: From microhydrodynamics to transport properties in microfluidic channels," thesis, UPMC (2016).
21. N. Figueroa-Morales, R. Soto, G. Junot, T. Darnige, C. Douarche, V. Martinez, A. Lindner, E. Clément, 3D spatial exploration by *E. coli* echoes motor temporal variability. arXiv:1803.01295 [physics.bio-ph] (4 March 2018).
22. G. Ariel, A. Rabani, S. Benisty, J. D. Partridge, R. M. Harshey, A. Be'er, Swarming bacteria migrate by Lévy Walk. *Nat. Commun.* **6**, 8396 (2015).
23. M. C. Marchetti, J. F. Joanny, S. Ramaswamy, T. B. Liverpool, J. Prost, M. Rao, R. Aditi Simha, Hydrodynamics of soft active matter. *Rev. Mod. Phys.* **85**, 1143 (2013).
24. F. Matthäus, M. S. Mommer, T. Curk, J. Dobnikar, On the origin and characteristics of noise-induced Lévy walks of *E. coli*. *PLOS ONE* **6**, e18623 (2011).
25. M. W. Sneddon, W. Pontius, T. Emonet, Stochastic coordination of multiple actuators reduces latency and improves chemotactic response in bacteria. *Proc. Natl. Acad. Sci. U.S.A.* **109**, 805–810 (2012).
26. J. Saragosti, V. Calvez, N. Bournaveas, B. Perthame, A. Buguin, P. Silberzan, Directional persistence of chemotactic bacteria in a traveling concentration wave. *Proc. Natl. Acad. Sci. U.S.A.* **108**, 16235–16240 (2011).
27. X. Fu, S. Kato, J. Long, H. H. Mattingly, C. He, D. C. Vural, S. W. Zucker, T. Emonet, Spatial self-organization resolves conflicts between individuality and collective migration. *Nat. Commun.* **9**, 2177 (2018).
28. D. J. Griffiths, Flow of urine through the ureter: A collapsible, muscular tube undergoing peristalsis. *J. Biomech. Eng.* **111**, 206–211 (1989).
29. K. J. Mullins, R. G. Saacke, Study of the functional anatomy of bovine cervical mucosa with special reference to mucus secretion and sperm transport. *Anat. Rec.* **225**, 106–117 (1989).
30. T. P. Kinney, Management of ascending cholangitis. *Gastrointest. Endosc. Clin. N. Am.* **17**, 289–306 (2007).

E. coli "super-contaminates" narrow ducts fostered by broad run-time distribution

Nuris Figueroa-Morales, Aramis Rivera, Rodrigo Soto, Anke Lindner, Ernesto Altshuler and Éric Clément

ARTICLE TOOLS	http://advances.sciencemag.org/content/6/11/eaay0155
SUPPLEMENTARY MATERIALS	http://advances.sciencemag.org/content/suppl/2020/03/09/6.11.eaay0155.DC1
REFERENCES	This article cites 27 articles, 6 of which you can access for free http://advances.sciencemag.org/content/6/11/eaay0155#BIBL
PERMISSIONS	http://www.sciencemag.org/help/reprints-and-permissions

Use of this article is subject to the Terms of Service